

Level structure of the ^{93}Nb nucleus and systematics of features in neighboring nuclei

Yi-Heng Wu ^{1,2}, Jing-Bin Lu,^{1,*} Zhen Ren,¹ Guan-Jian Fu ³, Jian Li,¹ Ke-Yan Ma,¹ Ying-Jun Ma,¹
Xiao-Guang Wu,⁴ Yun Zheng,⁴ Cong-Bo Li,⁴ and Jun Wen²

¹College of Physics, Jilin University, Changchun 130012, China

²School of Electronic Engineering and Intelligent Manufacturing, Anqing Normal University, Anqing 246133, China

³School of Physics Science and Engineering, Tongji University, Shanghai 200092, China

⁴China Institute of Atomic Energy, Beijing 102413, China



(Received 6 November 2021; revised 19 January 2022; accepted 14 March 2022; published 30 March 2022)

Excited states of the ^{93}Nb nucleus are produced through the fusion-evaporation reactions $^{82}\text{Se} (^{14}\text{N}, 3n) ^{93}\text{Nb}$ and $^{82}\text{Se} (^{16}\text{O}, 1p4n) ^{93}\text{Nb}$. On the basis of new experimental data, the previously known level scheme is extended. Level structure is discussed in comparison to a shell-model calculation. The calculation results demonstrate that the low-lying states can be interpreted as the excitation of the protons from the $1p_{1/2}$ orbit, through the $Z = 40$ subshell closure, to the $0g_{9/2}$ orbit. The moderate-spin states involve not only the proton excitation through the $Z = 38$ or 40 subshell ($0f_{5/2}1p_{3/2}1p_{1/2} \rightarrow 0g_{9/2}$), but also the neutron excitation through the $N = 56$ subshell ($1d_{5/2} \rightarrow 0g_{7/2}$). For the high-spin states above 9.1 MeV, the neutron excitation across the $N = 50$ closed shell plays a dominant role.

DOI: [10.1103/PhysRevC.105.034344](https://doi.org/10.1103/PhysRevC.105.034344)

I. INTRODUCTION

The level schemes of nuclei in the proximity of $Z = 38$ ($Z = 40$) subshell gap and $Z = 40$ shell gap have been widely studied in both experiments and theories [1–14]. These researches provide the opportunities to understand and explore the effects of $Z = 38$ ($Z = 40$) subshell gap and $N = 50$ shell gap on the level structures, particularly at high spins. For example, ^{92}Zr , ^{93}Nb , ^{94}Mo , ^{95}Tc , and ^{96}Ru possess a few valence nucleons above $Z = 38$ ($Z = 40$) subshell and $N = 50$ closed shell. The low-lying states can be described by the shell model with a ^{78}Ni core in which the valence protons are in the $p_{3/2}p_{1/2}f_{5/2}g_{9/2}$ orbits. For the states with high spins or high excitation energies, the core breaking of the $N = 50$ shell closure is an essential in generating angular momentum.

However, up to present, there has been relatively little experiment information on the level structures of nuclei with $52 \leq N \leq 54$ at high spins. Hence, the investigations of high spin states would provide new information important for understanding the mechanisms responsible for the generation of additional excitations. For example, neutron excitations from $d_{5/2}$ orbit, through the $N = 56$ subshell, to $g_{7/2}$ orbit coupled to the proton excitations within the $p_{3/2}p_{1/2}f_{5/2}g_{9/2}$ orbitals play a critical part in interpreting the level structures of these nuclei [1,5,6].

The level structure of ^{93}Nb has been investigated by different kinds of experimental measurements, such as β decay of $21/2^+$ Mo, $^{90}\text{Zr}(\alpha, p\gamma)$, $^{91}\text{Zr}(\alpha, d)$, $^{93}\text{Nb}(n, n'\gamma)$, the $^{94}\text{Zr}(p, 2n\gamma\gamma) ^{93}\text{Nb}$ and the nuclear resonance fluorescence method [15–19]. In Ref. [16], the 156-, 385-, 541-, 573-, 689-,

845-, 950-, 1262-, and 1418-keV γ rays were confirmed in the present paper. The 950-keV $13/2^+$ level has been observed in $^{90}\text{Zr}(\alpha, p\gamma)$. The 1335-keV $17/2^+$ level was known to decay by a single 385-keV γ ray, and the 1491-keV $15/2^+$ level was known to be depopulated by a 541-keV γ ray. Levels of ^{93}Nb have also been studied by the $^{82}\text{Se} (^{16}\text{O}, p4n)$ reaction [20], and the level scheme was extended up to the state at about 11 MeV [20]. Notwithstanding, the information on the structure of the ^{93}Nb nucleus is relatively lacking, in contrast to the detailed studies on high-spin states in the neighboring $Z = 41$ isotopes $^{90-92}\text{Nb}$ and the $N = 52$ isotones ^{92}Zr and ^{94}Mo [1,2,5,6,13,14].

The study of the high-spin states of ^{93}Nb is a follow-on effort to systematically study the level structures at high spins of nuclei in $A \approx 90$ ($Z \approx 38$, $N \approx 50$) mass region. One might expect that the further investigation on levels of ^{93}Nb would offer more rich and useful information about the proton $Z = 38$ ($Z = 40$) and neutron $N = 50$ ($N = 56$) core breaking mechanisms. Moreover, one finds the Nb isotopes evolve from spherical to deformed shapes as the neutron number increases. It is, therefore, the purpose of this paper to revisit ^{93}Nb by the fusion-evaporation reaction.

II. EXPERIMENTS AND RESULTS

Levels in ^{93}Nb were populated using a $^{82}\text{Se} (^{14}\text{N}, 3n) ^{93}\text{Nb}$ reaction at an incident beam energy of 54 MeV. The ^{14}N beam was delivered by the HI-13 tandem accelerator at the China Institute of Atomic Energy in Beijing. The target consisted of a 0.99-mg/cm² foil of ^{82}Se (isotopically enriched to 96%) evaporated on a 8.27-mg/cm² natural Yb backing. The de-excitation γ rays from the reaction residues were detected with an array comprising nine Compton-suppressed HPGe

*ljb@jlu.edu.cn

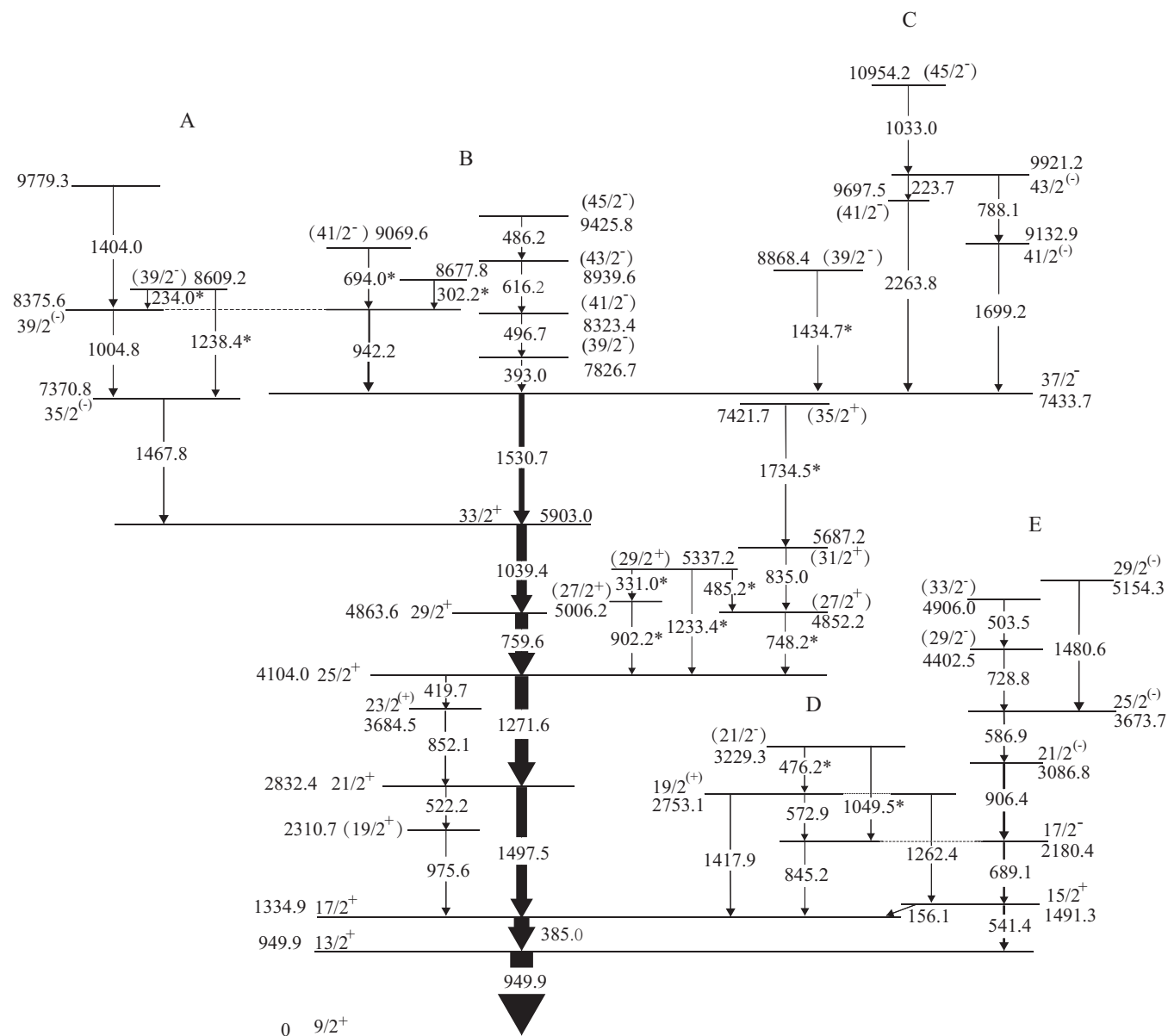


FIG. 1. Level scheme of ^{93}Nb obtained from the present paper, the energies are labeled in keV. Newly observed transitions are marked with black asterisks. The widths of the arrows denote the observed intensities.

detectors and two planar HPGe detectors centering around the target chamber. The energy and efficiency calibration of the detectors were performed using the standard radioactive sources of ^{60}Co , ^{133}Ba , and ^{152}Eu placed at the target position. The total of 150×10^6 γ - γ coincidence events were recorded. Events corresponding to γ rays emitted from the decay of excited nuclear states were sorted offline into two-dimensional symmetrized $E\gamma$ - $E\gamma$ coincidence matrices and two asymmetrized angular distribution from oriented (ADO) matrices (γ -ray angular distribution from oriented nuclei). The asymmetrized matrices were created by sorting the detectors at all angles (y axis) against those lying at θ_1 (40° and 152°) and θ_2 (90°) (x axes). Coincidence data were recorded when, at least, two signals from HPGe detectors were generated in 60 ns. For the level spin and parity assignments we used

ADO ratios with the definition $I_\gamma(\theta_1)/I_\gamma(\theta_2)$. Here the $I_\gamma(\theta_1)$ and $I_\gamma(\theta_2)$ correspond to the γ -ray intensities observed by detectors at either θ_1 or θ_2 obtained from the asymmetrized matrices respectively. With this definition, the ADO ratios for the stretched quadrupole or $\Delta I = 0$ dipole radiations and stretched pure dipole transitions are found to be ≈ 1.4 and 0.7, respectively, which are confirmed by the known γ -ray multiplicities. The states of ^{93}Nb were also populated by the $^{82}\text{Se}(^{16}\text{O}, p4n)^{93}\text{Nb}$ reaction. The target thickness is 2.5 mg/cm^2 with 90% enriched ^{82}Se evaporated on the $500\text{-}\mu\text{g/cm}^2$ -thick Au backing.

The level scheme of ^{93}Nb constructed from the present experiments is shown in Fig. 1. The placement of γ rays in the level scheme is based upon their coincidence relationships, energy sums, and intensity balances. Spin and parity

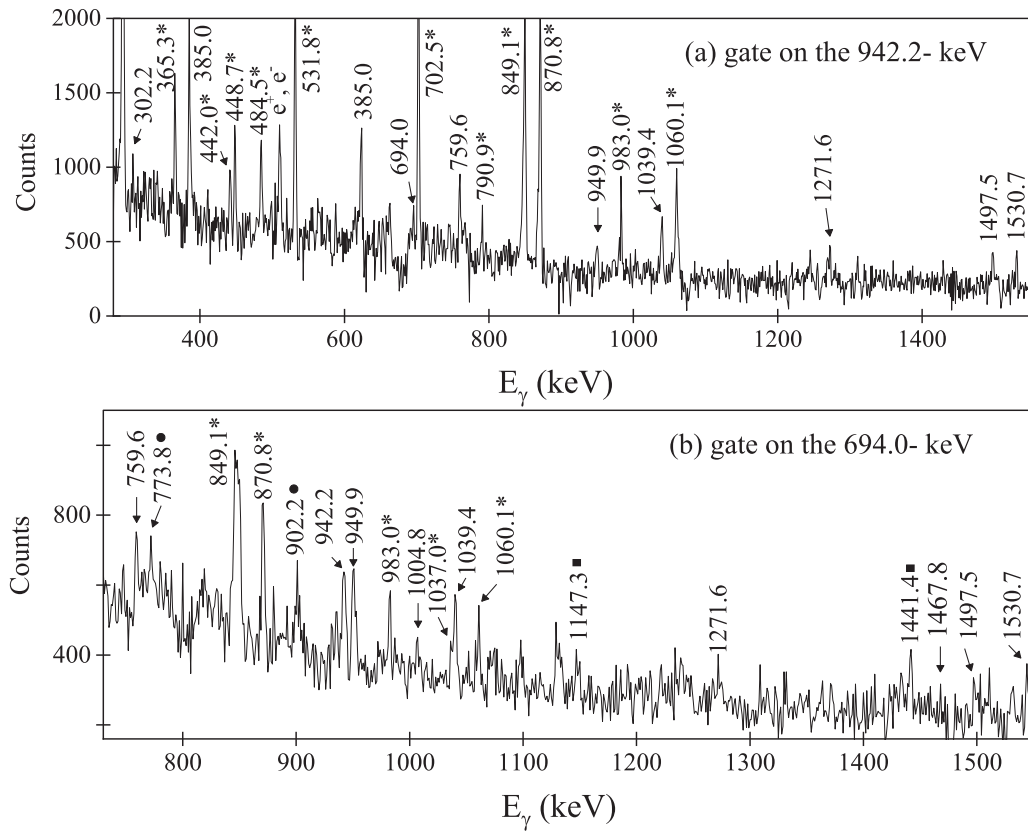


FIG. 2. Representative prompt γ - γ coincidence spectra of ^{93}Nb by using the $^{82}\text{Se} (^{16}\text{O}, 1p4n) ^{93}\text{Nb}$ reaction. (a) Gating on 942.2 keV [the energies with single asterisks are contaminations from the reaction channel $^{82}\text{Se} (^{16}\text{O}, 4n) ^{94}\text{Mo}$]; (b) gating on 694.0 keV [the energies with single asterisks, black circles, or black squares are contaminations from the reaction channel $^{82}\text{Se} (^{16}\text{O}, 4n) ^{94}\text{Mo}$, $^{82}\text{Se} (^{16}\text{O}, 3n) ^{95}\text{Mo}$ or $^{82}\text{Se} (^{16}\text{O}, 5n) ^{93}\text{Mo}$, respectively].

assignments are on the basis of γ - γ directional correlations and deexcitation modes. Relative intensities, γ -ray energies, ADO ratios, and suggested spin-parity assignments are listed in Table I. The typical coincidence γ -ray spectra gated on the transitions of ^{93}Nb are shown in Figs. 2–4.

The cascade of γ rays labeled A in Fig. 1, two new transitions 234.0 and 1238.4 (234.0 + 1004.8) keV belonging to ^{93}Nb were identified. The 1238.4-keV transition is in coincidence with the 1467.8-, 1039.4-, 759.6-, and 1271.6-keV tran-

sitions but not coincidence with the 1004.8- and 234.0-keV transitions. The 234.0- and 1238.4-keV γ rays were placed on top of the $39/2^{-}$ state at 8375.6 keV and the $35/2^{-}$ state at 7370.8 keV as shown in Fig. 1.

As for transitions in group B, the 942-, 393-, 497-, 615-, and 486-keV transitions, reported in Ref. [20], are also observed in the present experiments. In addition, the new transitions 694.0 and 302.2 keV were placed above the $39/2^{-}$ state at 8375.6 keV. The transitions 694.0 and 302.2 keV were

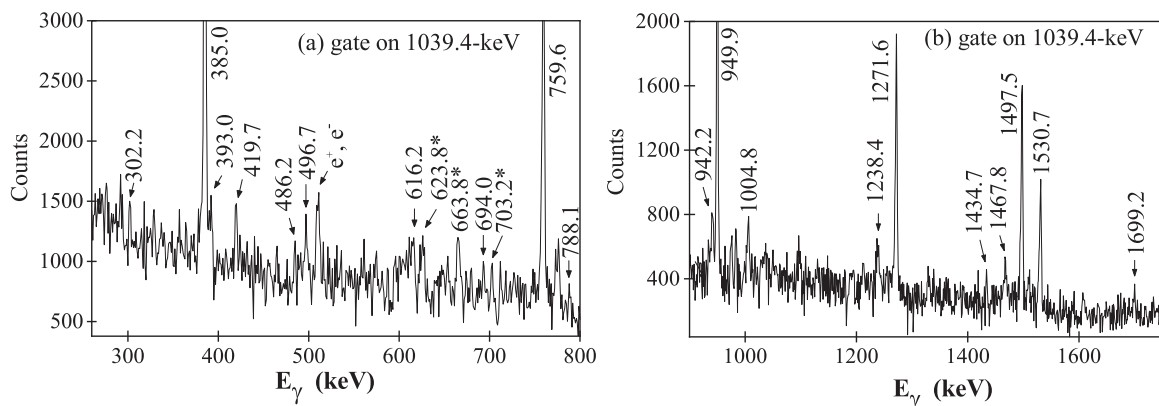


FIG. 3. Representative prompt γ - γ coincidence spectra of ^{93}Nb by using the $^{82}\text{Se} (^{16}\text{O}, 1p4n) ^{93}\text{Nb}$ reaction. The energies with single asterisks or black squares are contamination from the reaction channel $^{82}\text{Se} (^{16}\text{O}, 4n) ^{94}\text{Mo}$. γ rays are labeled with their energies in keV.

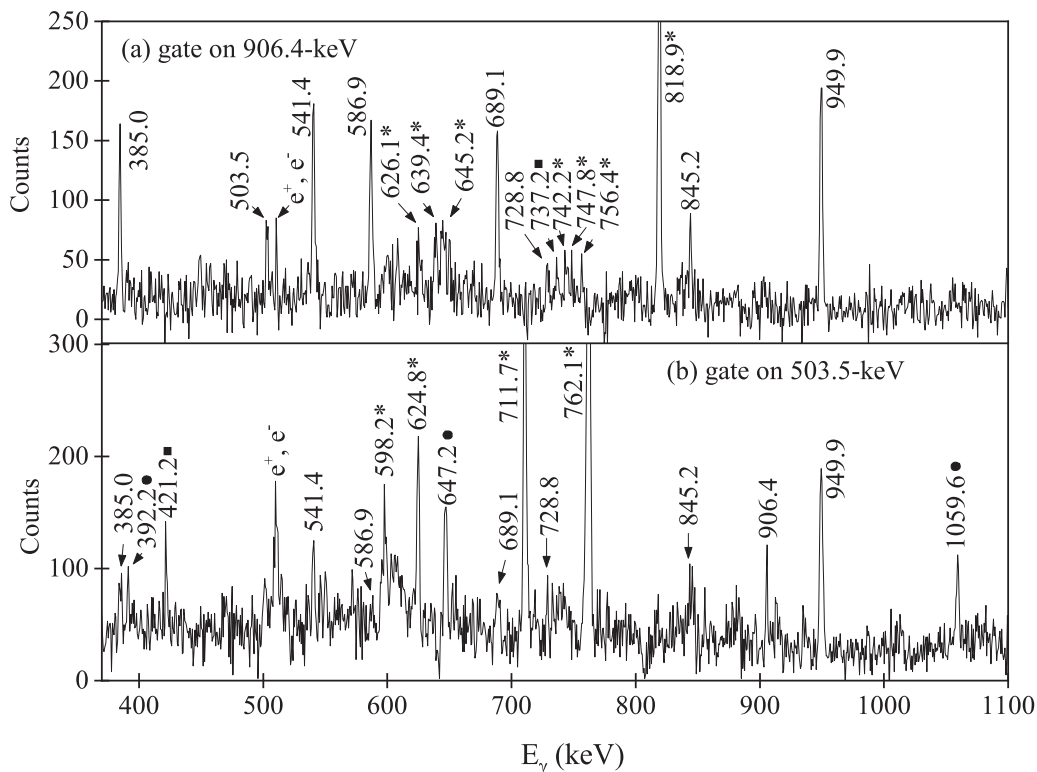


FIG. 4. Representative prompt γ - γ coincidence spectra of ^{93}Nb by using the $^{82}\text{Se}(^{14}\text{N}, 3n)^{93}\text{Nb}$ reaction. (a) Gating on 906.4 keV (the energies with single asterisks or black squares are contamination from are contamination from the reaction channel $^{82}\text{Se}(^{14}\text{N}, 5n)^{91}\text{Nb}$ or $^{82}\text{Se}(^{14}\text{N}, 4n)^{92}\text{Nb}$, respectively); (b) gating on 503.5 keV (the energies with single asterisks, black circles, or black squares are contamination from the reaction channel $^{82}\text{Se}(^{14}\text{N}, 4n)^{92}\text{Nb}$, $^{82}\text{Se}(^{14}\text{N}, p2n)^{93}\text{Zr}$ or $^{82}\text{Se}(^{14}\text{N}, 5n)^{91}\text{Nb}$, respectively). γ rays are labeled with their energies in keV.

found to be in coincidence with the 942.2-, 1530.7-, 1039.4-, and 1271.6-keV transitions, whereas the 694.0-keV transition is not in coincidence with 302.2 keV. As can be seen from Figs. 2(a) and 3, the 694.0- and 302.2-keV transitions can be observed from the γ -ray coincidence spectra gated on the 942.2- and 1039.4-keV transitions and the known transitions 759.6-, 942.2-, 949.9-, 1039.4-, 1271.6-, and 1497.5-keV transitions can be also observed from the 694.0-keV γ -ray coincidence spectrum. It is important to note that there are several strong peaks (i.e., 773.8, 849.1, 870.8, 902.2, 983.0, 1037.0, and 1060.1 keV) in the 694.0-keV γ -ray coincidence spectrum. From the analysis of the present data, we found that the 773.8-, 849.1-, 870.8-, 902.2-, 983.0-, 1037.0-, and 1060.1-keV γ rays from ^{94}Mo are also coincidence with 695.0-keV γ rays, although they were not observed in Ref. [6].

In group C, a newly observed 1434.7-keV γ ray is assigned to feed the $37/2^-$ state (7433.7-keV level). In the spectra gated by the 1039.4-keV γ ray, the 1434.7-keV γ ray is observed, but in the spectra gated by the 942.2-keV γ ray, the 1434.7-keV γ ray is absent. After careful analyses, we confirmed that 1434.7-keV γ ray is assigned to ^{93}Nb .

Moreover, in the present paper the multipolarities of 942.2- and 1004.8-keV γ rays are assigned as $\Delta I = 1$ and $\Delta I = 2$, respectively, which are different from what was proposed in Ref. [20] where the 942.2- and 1004.8-keV γ rays were assigned as $\Delta I = 0$ and $\Delta I = 1$, respectively. We tentatively

proposed the energy level 8375.6 keV as $39/2^-$, which is $1\hbar$ larger than that from Ref. [20].

The low-lying part of the level scheme labeled D, in Ref. [15], the 156.1-, 845.2-, 572.9-, 1417.9-, and 1262.4-keV transitions are confirmed in this paper, although they were not observed in Ref. [20]. The new transitions 476.2 and 1049.5 keV belonging to ^{93}Nb are added. In Ref. [2], the 503.5 keV is added to the level scheme of ^{93}Nb feeding into the $17/2^-$ (2180.4-keV level), however, the 503.5 keV is assigned to feed the $(29/2^-)$ (4402.5-keV level) in our paper. In the coincidence spectrum gated on the 906.4-keV transition [shown in Fig. 4(a)], the known transitions 385.0, 541.4, 689.1, 586.9, and 728.8 keV as well as the transition 503.5 keV are observed. As shown in Fig. 4(b), the 385.0-, 541.4-, 586.9-, 689.1-, 728.8-, and 906.4-keV transitions are displayed in the gated spectrum of the 503.5-keV transition. From the analyses of intensity balance and the coincidence relationships with 541.4-, 586.9-, 689.1-, 728.8-, and 949.9-keV transitions, the 503.5-keV transition is placed on top of the $29/2^-$ (4402.5-keV level).

In addition, the new 331.0-, 485.2-, 748.2-, 902.2-, 1233.4-, and 1734.5-keV γ rays belonging to ^{93}Nb are identified and found to be in coincidence with the 1271.6-, 1497.5-, 385.0-, and 949.9-keV transitions, but not with the 759.6- and 1039.4-keV transitions. These γ rays are placed on top of the $25/2^+$ state at 4104.0 keV as given in Fig. 1.

TABLE I. γ -ray energies, relative intensities, ADO ratios, initial, and final state spins, and initial and final E_γ , of transitions assigned to ^{93}Nb in the present experiment.

E_γ^a	I_γ^b	R_{ADO}	E_i^π	E_f^π	J_i^π	J_f^π
156.1	4.03(40)	0.97(30)	1491.3	1334.9	15/2 ⁺	17/2 ⁺
223.7	4.40(85)		9921.2	9697.5	43/2 ⁽⁻⁾	(41/2 ⁻)
234.0			8609.2	8375.6	(39/2 ⁻)	39/2 ⁽⁻⁾
302.2	7.05(85)		8677.8	8375.6		39/2 ⁽⁻⁾
331.0			5337.2	5006.2	(29/2 ⁺)	(27/2 ⁺)
385.0	100	1.87(23)	1334.9	949.9	17/2 ⁺	13/2 ⁺
393.0	7.43(92)	1.08(28)	7826.7	7433.7	(39/2 ⁻)	37/2 ⁻
419.7	7.93(43)	1.09(20)	4104.0	3684.5	25/2 ⁺	23/2 ⁽⁺⁾
476.2	6.47(81)		3229.3	2753.1	(21/2 ⁻)	19/2 ⁽⁺⁾
485.2			5337.2	4852.2	(29/2 ⁺)	(27/2 ⁺)
486.2	4.34(47)		9425.8	8939.6	(45/2 ⁻)	(43/2 ⁻)
496.7	6.74(46)		8323.4	7826.7	(41/2 ⁻)	(39/2 ⁻)
503.5	5.42(63)	1.38(28)	4906.0	4402.5	(33/2 ⁻)	(29/2 ⁻)
522.2	4.20(29)		2832.4	2310.7	21/2 ⁺	(19/2 ⁺)
541.4	19.83(86)	0.81(16)	1491.3	949.9	15/2 ⁺	13/2 ⁺
572.9	8.80(85)		2753.1	2180.4	19/2 ⁽⁺⁾	17/2 ⁻
586.9	14.74(83)	1.47(26)	3673.7	3086.8	25/2 ⁽⁻⁾	21/2 ⁽⁻⁾
616.2	6.74(46)		8939.6	8323.4	(43/2 ⁻)	(41/2 ⁻)
689.1	18.71(91)	0.96(24)	2180.4	1491.3	17/2 ⁻	15/2 ⁺
694.0			9069.6	8375.6	(41/2 ⁻)	39/2 ⁽⁻⁾
728.8	6.45(83)		4402.5	3673.7	(29/2 ⁻)	25/2 ⁽⁻⁾
748.2			4852.2	4104.0	(27/2 ⁺)	25/2 ⁺
759.6	106.2(2.4)	1.36(19)	4863.6	4104.0	29/2 ⁺	25/2 ⁺
788.1	4.73(94)		9921.2	9132.9	43/2 ⁽⁻⁾	41/2 ⁽⁻⁾
835.0			5687.2	4852.2	(31/2 ⁺)	(27/2 ⁺)
845.2	13.80(93)	1.51(17)	2180.4	1334.9	17/2 ⁻	17/2 ⁺
852.1	12.10(63)	0.92(16)	3684.5	2832.4	23/2 ⁽⁺⁾	21/2 ⁺
902.2			5006.2	4104.0	(27/2 ⁺)	25/2 ⁺
906.4	25.42(100)	1.55(22)	3086.8	2180.4	21/2 ⁽⁻⁾	17/2 ⁻
942.2	11.23(97)	0.67(8)	8375.6	7433.7	39/2 ⁽⁻⁾	37/2 ⁻
949.9	155.10(500)	1.68(27)	949.9	0	13/2 ⁺	9/2 ⁺
975.6	4.09(35)	0.81(21)	2310.7	1334.9	(19/2 ⁺)	17/2 ⁺
1004.8	11.20(120)	1.86(19)	8375.6	7370.8	39/2 ⁽⁻⁾	35/2 ⁽⁻⁾
1033.0			10954.2	9921.2	(45/2 ⁻)	43/2 ⁽⁻⁾
1039.4	77.20(200)	1.53(18)	5903.0	4863.6	33/2 ⁺	29/2 ⁺
1049.5			3229.3	2180.4	(21/2 ⁻)	17/2 ⁻
1233.4			5337.2	4104.0	(29/2 ⁺)	25/2 ⁺
1238.4			8609.2	7370.8	(39/2 ⁻)	35/2 ⁽⁻⁾
1262.4			2753.1	1491.3	19/2 ⁽⁺⁾	15/2 ⁺
1271.6	87.40(2.4)	1.31(21)	4104.0	2832.4	25/2 ⁺	21/2 ⁺
1404.0			9779.3	8375.6		39/2 ⁽⁻⁾
1417.9	3.05(63)		2753.1	1334.9	19/2 ⁽⁺⁾	17/2 ⁺
1434.7			8868.4	7433.7	(39/2 ⁻)	37/2 ⁻
1467.8	13.26(93)	0.80(13)	7370.8	5903.0	35/2 ⁽⁻⁾	33/2 ⁺
1480.6	7.17(72)	1.25(24)	5154.3	3673.7	29/2 ⁽⁻⁾	25/2 ⁽⁻⁾
1497.5	77.40(230)	1.59(31)	2832.4	1334.9	21/2 ⁺	17/2 ⁺
1530.7	37.86(400)	1.83(22)	7433.7	5903.0	37/2 ⁻	33/2 ⁺
1699.2	7.58(120)		9132.9	7433.7	41/2 ⁽⁻⁾	37/2 ⁻
1734.5			7421.7	5687.2	(35/2 ⁺)	(31/3 ⁺)
2263.8	< 2		9697.5	7433.7	(41/2 ⁻)	37/2 ⁻

^aThe uncertainty in strong γ -ray energies is less than 0.4 keV; for weak γ -ray energies, it is about 0.7 keV.

^bIntensities are corrected for detector efficiency and normalized to 100 for the 385.0-keV transition.

III. SHELL-MODEL CALCULATIONS AND DISCUSSION

The ^{93}Nb isotones ^{90}Sr [21], ^{91}Y [10], ^{94}Mo [6], ^{95}Tc [22], and the isotopes $^{91,92,94}\text{Nb}$ [3,13,23] were investigated systematically by the shell model. These studies demonstrate that promoting protons from the $1p0f$ orbits into the $0g_{9/2}$ orbit is sufficient to describe the low-spin states. For high-spin states, the neutron core excitation through the $N = 50$ shell closure is proposed to be considered. In this paper, we consider ^{93}Nb in the $\pi 0f_{5/2}1p_{3/2}1p_{1/2}0g_{9/2}$ and $\nu 1p_{1/2}0g_{9/2}1d_{5/2}g_{7/2}$ shells in our shell-model calculation. The NUSHELLX code is used with the GWBXC effective interaction [24]. In our calculations, the single particle energies (SPEs) (in MeV) corresponding to the model space were set as $\epsilon_{f_{5/2}}^\pi = -5.322$, $\epsilon_{p_{3/2}}^\pi = -6.144$, $\epsilon_{p_{1/2}}^\pi = -3.941$, $\epsilon_{g_{9/2}}^\pi = -1.250$, $\epsilon_{p_{1/2}}^\nu = -0.696$, $\epsilon_{g_{9/2}}^\nu = -2.597$, $\epsilon_{g_{7/2}}^\nu = +5.159$, and $\epsilon_{d_{5/2}}^\nu = +1.830$.

One sees about a 4.0 (2.7)-MeV SPE gap between the $f_{5/2}$ ($p_{1/2}$) and the $g_{9/2}$ orbits for the valence protons, which indicates the possible $Z = 38$ (40) subshell. For the valence neutrons, the SPE gap of the $N = 50$ shell closure is 4.4 MeV and that between the $d_{5/2}$ and $g_{7/2}$ orbits is 3.3 MeV, which might support the existence of the $N = 56$ subshell.

We truncate the shell-model space of ^{93}Nb with both proton and neutron particle-hole excitations across the ^{90}Zr core, i.e., the valence proton holes are in the lower $f_{5/2}p_{3/2}p_{1/2}$ orbits, the valence proton particles are in the upper $g_{9/2}$ orbit, the valence neutron holes are in the lower $p_{1/2}g_{9/2}$ orbits, and the valence neutron particles are in the upper $d_{5/2}g_{7/2}$ orbits. The proton particle-hole excitation across the $Z = 40$ subshell is up to $2p2h$, and, at most, one neutron in the lower $g_{9/2}$ orbit is permitted to be excited into the upper $d_{5/2}g_{7/2}$ orbits.

Figure 5 compares the level energies from experiments and the shell-model calculations. Dominant configurations of the wave functions are presented in Table II. As shown in Fig. 5, the calculated results are in good agreement with the experimental data. Let us begin our discussion with the positive-parity states. From Table II, the $9/2^+$ ground state mainly stems from a $g_{9/2}$ proton. The $13/2^+$, $15/2^+$, and $17/2^+$ states are predicted to contain both the $\pi(p_{1/2})^{-2}g_{9/2}^3 \otimes \nu d_{5/2}^2$ and the $\pi g_{9/2} \otimes \nu d_{5/2}^2$ configuration components. The observed $15/2^+$ (1491-keV level) state lies above $17/2^+$ (1335-keV level) state, and our shell-model calculation well reproduces this phenomenon. The states with $2300 < E_{\text{exp}} < 6000$ keV (except for the $29/2_2^+$ state) mainly involve the configuration $\pi(f_{5/2}p_{1/2}p_{3/2})^{-2}g_{9/2}^3 \otimes \nu d_{5/2}g_{7/2}$ in which a valence neutron from the $d_{5/2}$ orbit is excited across the $N = 56$ subshell to the $g_{7/2}$ orbit. The $29/2_2^+$ state originates from the promotion of one neutron pair from the $d_{5/2}$ orbit to the $g_{7/2}$ orbit, leading to the main configuration $\pi p_{1/2}^{-2}g_{9/2}^3 \otimes \nu g_{7/2}^2$. For the state with $35/2^+$, the main configuration in the wave functions is $\pi(f_{5/2}^{-1}p_{1/2}^{-1}g_{9/2}^3) \otimes \nu g_{7/2}^2$.

Now we come to the negative-parity states. The dominant configuration in the $17/2^-$ and $21/2_1^-$ states is $\pi p_{1/2}^{-1}g_{9/2}^2 \otimes \nu d_{5/2}^2$. The calculated $21/2_2^-$ state includes mainly the configuration $\pi p_{1/2}^{-1}g_{9/2}^2 \otimes \nu d_{5/2}g_{7/2}$. Most of the $25/2^- \leq J^\pi \leq 37/2^-$ states are interpreted by the

EXP (A)	SM	EXP (B)	SM	EXP (C)	SM	EXP (E)	SM
				<u>45/2⁻ 10954.2</u>	<u>45/2⁻ 10511</u>		
				<u>43/2⁻ 9921.2</u>	<u>43/2⁻ 9995</u>		
		<u>45/2⁻ 9425.8</u>	<u>45/2⁻ 9514</u>	<u>41/2⁻ 9697.5</u>	<u>41/2⁻ 9535</u>		
		<u>41/2⁻ 9069.6</u>	<u>41/2⁻ 9103</u>	<u>41/2⁻ 9132.9</u>	<u>41/2⁻ 9206</u>		
<u>39/2⁻ 8609.2</u>	<u>39/2⁻ 8626</u>	<u>43/2⁻ 8939.6</u>	<u>43/2⁻ 8924</u>	<u>39/2⁻ 8868.4</u>	<u>39/2⁻ 8734</u>		
<u>39/2⁻ 8375.3</u>	<u>39/2⁻ 8096</u>	<u>41/2⁻ 8323.4</u>	<u>41/2⁻ 8542</u>				
<u>35/2⁻ 7370.8</u>	<u>35/2⁻ 7093</u>	<u>39/2⁻ 7826.7</u>	<u>39/2⁻ 7787</u>	<u>33/2⁺ 7421.7</u>			
		<u>37/2⁻ 7433.7</u>	<u>37/2⁻ 7309</u>		<u>33/2⁺ 7082</u>		
		<u>33/2⁺ 5903.0</u>	<u>33/2⁺ 5741</u>	<u>31/2⁺ 5687.2</u>	<u>31/2⁺ 5593</u>		
				<u>29/2⁺ 5337.2</u>	<u>29/2⁺ 5199</u>	<u>29/2⁻ 5154.3</u>	<u>29/2⁻ 5341</u>
		<u>29/2⁺ 4863.6</u>	<u>29/2⁺ 4973</u>	<u>27/2⁺ 5006.2</u>	<u>27/2⁺ 4978</u>	<u>33/2⁻ 4906.0</u>	<u>29/2⁻ 5329</u>
				<u>27/2⁺ 4852.8</u>	<u>27/2⁺ 4616</u>	<u>29/2⁻ 4402.5</u>	<u>29/2⁻ 4441</u>
		<u>25/2⁺ 4104.0</u>	<u>25/2⁺ 3929</u>	EXP (D)	SM	<u>25/2⁻ 3673.7</u>	<u>25/2⁻ 3654</u>
		<u>23/2⁺ 3684.5</u>	<u>23/2⁺ 3581</u>	<u>27/2⁺ 3229.3</u>	<u>27/2⁺ 3535</u>	<u>21/2⁻ 3086.8</u>	<u>21/2⁻ 3375</u>
		<u>21/2⁺ 2832.4</u>	<u>21/2⁺ 3007</u>	<u>19/2⁺ 2753.1</u>	<u>19/2⁺ 2948</u>		
		<u>19/2⁺ 2310.7</u>	<u>19/2⁺ 1987</u>			<u>17/2⁻ 2180.4</u>	<u>17/2⁻ 2311</u>
			<u>17/2⁺ 1426</u>			<u>15/2⁺ 1491.3</u>	<u>15/2⁺ 1544</u>
		<u>17/2⁺ 1334.9</u>	<u>17/2⁺ 1426</u>				
		<u>13/2⁺ 949.9</u>	<u>13/2⁺ 923</u>				
		<u>9/2⁺ 0</u>	<u>9/2⁺ 0</u>				

FIG. 5. Comparison of the experimental levels and the calculated levels of ^{93}Nb .

configuration $\pi(f_{5/2}p_{3/2}p_{1/2})^{-3}g_{9/2}^4 \otimes \nu d_{5/2}g_{7/2}$. The $39/2_1^-$ and $39/2_2^-$ states are characterized by proton excitation from the $f_{5/2}p_{3/2}p_{1/2}$ orbits to the $g_{9/2}$ orbit coupled a neutron pair excitation from the $d_{5/2}$ orbit, through the $N = 56$ subshell, to the $g_{7/2}$ orbit, viz., configuration of the form $\pi(f_{5/2}^{-1}p_{1/2}^{-2})g_{9/2}^4 \otimes \nu g_{7/2}^2$. The states with $8600 < E_{\text{exp}} < 9000$ keV are characterized by proton excitation from the $f_{5/2}p_{3/2}p_{1/2}$ orbits to the $g_{9/2}$ orbit coupled a neutron excitation from the $d_{5/2}$ orbit, through the $N = 56$ subshell, to the $g_{7/2}$ orbit, i.e., configuration of the form $\pi(f_{5/2}p_{3/2}p_{1/2})^{-3}g_{9/2}^4 \otimes \nu d_{5/2}g_{7/2}$.

For the $41/2_3^-$, $41/2_4^-$, $43/2_2^-$, and $45/2_2^-$ states, whose excitation energies are larger than 9100 keV, the particle-hole excitation across the $N = 50$ shell closure plays a significant role, and the main configuration in the wave function is $\pi(f_{5/2}p_{3/2}p_{1/2})^{-3}g_{9/2}^4 \otimes \nu g_{9/2}^{-1}d_{5/2}g_{7/2}^2$. The neutron core excitation of the $N = 50$ shell closure appears first at $41/2_1^-$ (9132.9 keV). At this level energy, it is more favorable for ^{93}Nb to generate angular momentum by breaking the $N = 50$ neutron core than by exciting more protons to the $g_{9/2}$ orbit.

IV. THE SYSTEMATIC FEATURES WITH NEIGHBORING NUCLEI

Figures 6(a) and 6(b) exhibit the systematics of the 0_1^+ , 2_1^+ , and 4_1^+ states in the even-even Zr isotopes and the $9/2_1^+$, $13/2_1^+$, and $17/2_1^+$ states in the odd-A Nb isotopes, respectively. The resemblance of the level schemes between the

odd-A Nb isotopes and the neighboring even-even Zr isotopes is conspicuous, up to the 4_1^+ state. For example, the $13/2_1^+$ and $17/2_1^+$ states in ^{93}Nb , at 949.9 and 1334.9 keV, are close in energies to the 2_1^+ and 4_1^+ states at 935 and 1496 keV in the ^{92}Zr core. This may be interpreted by the weak coupling model.

In the simplified weak coupling model, low-lying states of an odd-mass nucleus are described by a single nucleon in a single- j orbit moving outside an even-even core. We use $\psi_j^\dagger|0\rangle$ to denote the wave function of the low-lying I_1^+ state of the core, whose energy is denoted as E_I . By coupling $\psi_j^\dagger|0\rangle$ with the single nucleon a_j^\dagger , one obtains the so-called multiplet states with spin J for the odd-mass nucleus,

$$(\psi_j^\dagger a_j^\dagger)_J|0\rangle, \quad (1)$$

where $J = |I - j|, |I - j| + 1, \dots, I + j$. We use $E_J(I, j)$ to denote the excitation energy of the multiplet states. The relation between E_I and $E_J(I, j)$ is given by

$$E_I = \frac{\sum_J (2J + 1)E_J(I, j)}{\sum_J 2J + 1}. \quad (2)$$

The configuration $\pi g_{9/2} \otimes (2_1^+, ^{92}\text{Zr})$ could produce multiplet states with $5/2_1^+$ (809 keV), $7/2_1^+$ (744 keV), $9/2_2^+$ (1083 keV), $11/2_1^+$ (979 keV), and $13/2_1^+$ (950 keV) in ^{93}Nb . Using Eq. (2), we obtain that the excitation energy of the 2_1^+ state in ^{92}Zr is 934 keV, which is in excellent agreement with the experiment result (934.5 keV) [1].

TABLE II. Main partitions of the wave functions for ^{93}Nb . The wave function for a particular angular momentum state would be composed of several partitions where each partition is of the form $p = \{\pi[p(1), p(2), p(3), p(4)] \otimes \nu[n(1), n(2), n(3), n(4)]\}$, where $p(i)$ represents the number of protons occupying the ($f_{5/2}$, $p_{3/2}$, $p_{1/2}$, $g_{9/2}$) orbits, and $n(j)$ represents the number of neutrons in the ($p_{1/2}$, $g_{9/2}$, $g_{7/2}$, $d_{5/2}$) orbits, respectively. In these calculations two neutrons from the $d_{5/2}$ orbit are allowed to be excited to the $g_{7/2}$ orbit.

I^π (\hbar)	$E_{(\text{exp})}$ (keV)	$E_{(\text{cal})}$ (keV)	Wave function $\pi \otimes \nu$	Partitions (%)
$9/2^+$	0	0	$6421 \otimes 21002$	29.30
			$6403 \otimes 21002$	17.47
$13/2^+$	949.9	923	$6403 \otimes 21002$	21.92
			$6421 \otimes 21002$	20.70
$15/2^+$	1491.3	1544	$6421 \otimes 21002$	43.81
			$6403 \otimes 21002$	16.08
$17/2^+$	1334.9	1426	$6421 \otimes 21002$	53.81
			$6403 \otimes 21002$	14.09
$19/2_1^+$	2310.7	1987	$6403 \otimes 21011$	29.84
			$6421 \otimes 21011$	17.84
$19/2_2^+$	2753.1	2948	$4423 \otimes 21011$	9.65
			$5413 \otimes 21011$	28.13
			$6403 \otimes 21011$	14.89
$21/2_1^+$	2832.4	3007	$5323 \otimes 21011$	9.24
			$5413 \otimes 21011$	39.22
			$5413 \otimes 21020$	10.40
$23/2^+$	3684.5	3581	$5413 \otimes 21011$	7.91
			$5413 \otimes 21011$	28.78
			$6313 \otimes 21011$	24.30
$25/2^+$	4104.0	3929	$5413 \otimes 21011$	36.28
			$6313 \otimes 21011$	11.57
$27/2_1^+$	4852.2	4616	$6403 \otimes 21011$	36.04
			$5413 \otimes 21011$	14.79
			$4423 \otimes 21011$	13.14
$27/2_2^+$	5006.2	4978	$5413 \otimes 21011$	43.25
			$5323 \otimes 21011$	15.74
$29/2_1^+$	4863.6	4973	$5413 \otimes 21011$	68.83
$29/2_2^+$	5337.2	5199	$6403 \otimes 21020$	23.59
			$6403 \otimes 21011$	16.08
$31/2^+$	5687.2	5593	$5413 \otimes 21011$	54.09
$33/2^+$	5903.0	5741	$5413 \otimes 21011$	72.09
$35/2^+$	7421.7	7082	$5413 \otimes 21020$	39.05
$17/2^-$	2180.4	2311	$6412 \otimes 21002$	65.07
			$5422 \otimes 21002$	6.97
$21/2_1^-$	3086.8	3375	$6412 \otimes 21002$	55.35
			$6322 \otimes 21002$	10.89
$21/2_2^-$	3229.3	3535	$6412 \otimes 21011$	52.24
			$5404 \otimes 21011$	33.88
$25/2^-$	3673.7	3654	$4414 \otimes 21011$	16.79
			$5314 \otimes 21011$	14.25
			$5404 \otimes 21011$	39.31
$29/2_1^-$	4402.5	4441	$5314 \otimes 21011$	14.44%
$29/2_2^-$	5154.3	5341	$5404 \otimes 21011$	28.83%
			$6322 \otimes 21011$	21.44
			$5422 \otimes 21011$	7.66
$33/2^-$	4906.0	5329	$5404 \otimes 21011$	33.26
			$5422 \otimes 21011$	21.03
			$4414 \otimes 21011$	11.34

TABLE II. (Continued.)

I^π (\hbar)	$E_{(\text{exp})}$ (keV)	$E_{(\text{cal})}$ (keV)	Wave function $\pi \otimes \nu$	Partitions (%)
$35/2^-$	7370.8	7093	$4414 \otimes 21011$	33.04
			$5404 \otimes 21011$	17.59
			$4324 \otimes 21011$	11.96
$37/2_1^-$	7433.7	7309	$5404 \otimes 21011$	34.76
			$4414 \otimes 21011$	18.04
			$5314 \otimes 21011$	18.01
$39/2_1^-$	7826.7	7787	$5404 \otimes 21020$	39.09
			$5314 \otimes 21020$	19.57
			$5404 \otimes 21020$	10.62
$39/2_2^-$	8375.3	8096	$5404 \otimes 21020$	26.75
			$4324 \otimes 21020$	15.58
$39/2_3^-$	8609.2	8626	$5314 \otimes 21020$	14.62
			$4414 \otimes 21011$	44.10
$39/2_4^-$	8868.4	8734	$4324 \otimes 21020$	12.72
			$5314 \otimes 21011$	42.39
$41/2_1^-$	8323.4	8542	$4414 \otimes 21020$	16.41
			$4414 \otimes 21011$	58.86
$41/2_2^-$	9069.6	9103	$4414 \otimes 21020$	10.10
			$4414 \otimes 21011$	43.78
$41/2_3^-$	9132.9	9206	$4324 \otimes 21020$	16.14
			$5404 \otimes 2921$	32.33
$41/2_4^-$	9697.5	9535	$5314 \otimes 2921$	10.94
			$5404 \otimes 2921$	34.15
$43/2_1^-$	8939.6	8924	$4414 \otimes 2921$	23.98
			$4414 \otimes 21011$	55.97
$43/2_2^-$	9921.2	9995	$4324 \otimes 21011$	27.24
			$5404 \otimes 2921$	33.38
$45/2_1^-$	9425.8	9514	$4414 \otimes 2921$	24.27
			$5314 \otimes 21020$	38.90
$45/2_2^-$	10954.2	10511	$5314 \otimes 21011$	36.80
			$5404 \otimes 2921$	36.42
			$5314 \otimes 2921$	16.00

Similarly, the configuration $\pi g_{9/2} \otimes (2_1^+, {}^{94}\text{Mo})$ produces multiplet states with $5/2_1^+$ (627 keV), $7/2_1^+$ (336 keV), $9/2_2^+$ (1213 keV), $11/2_1^+$ (975 keV), and $13/2_1^+$ (882 keV) in ^{95}Tc [22,31]. Using Eq. (2), one obtains that the excitation energy of the 2_1^+ state in ^{94}Mo is 848 keV, which is also very close to the data (872 keV) [12]. We note that the $13/2_1^+$ and $17/2_1^+$ states in ^{99}Nb have not been observed, but Ref. [28] reports the 2_1^+ (1224-keV) and 4_1^+ (1843-keV) states in ^{98}Zr . Based on the the weak coupling model, one would expect that the $13/2_1^+$ and $17/2_1^+$ states of ^{99}Nb can be observed at about 1.2 and 1.8 MeV, in future experiments.

Figure 6(c) compares the energy levels in the $N = 52$ odd- A and even-even isotones. The yrast $13/2^+$ and $17/2^+$ states in ^{93}Nb , ^{95}Tc , and ^{97}Rh are close in energies with the yrast 2^+ and 4^+ states in ^{92}Zr , ^{94}Mo , and ^{96}Ru , respectively [5,29,11–14]. The above results can be also interpreted by the weak coupling model, i.e., a valence nucleon coupled to the low-lying state of the neighboring even-even core. It is worth mentioning that high-spin states do not follow the scenario of the weak coupling model, for example, the $25/2_1^+$ state in ^{93}Nb and the 8_1^+ state in ^{92}Zr are not close in energy. The

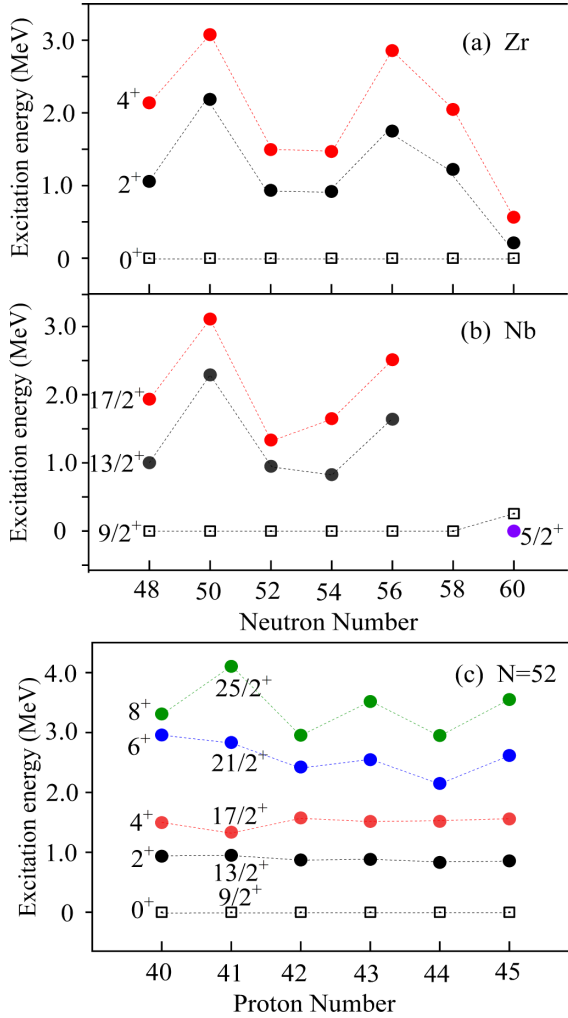


FIG. 6. (a) Comparison of the low-energy levels in the Zr isotopes [23–27]; (b) the same as (a) but for Nb isotopes [7,28–33]; (c) the evolution of the 0^+ , 2^+ , 4^+ , 6^+ , and 8^+ states in the even-even Zr isotones and the $9/2^+$, $13/2^+$, $17/2^+$, $21/2^+$, and 25^+ states in the odd-A Nb isotones [5,29,11–14].

reason is that the intrinsic nucleon excitations in high-spin states of the even-even core cannot be ignored, and configuration mixing becomes important.

In Figure 6(a) one sees the excitation energy ratio between the 4^+ and the 2^+ states in $^{90-98}\text{Zr}$ is smaller than 2, which indicates the stability of the $Z = 40$ subshell in these isotopes. In ^{100}Zr the excitation energy of the 2^+ drops significantly, and the low-lying spectrum follows the rotational behavior, which indicates the deformation onset in Zr isotopes with the increasing of neutrons beyond $N = 58$. We find the energy gap between the ground state and the first excited state is relatively larger in ^{90}Zr , ^{96}Zr , ^{91}Nb , and ^{97}Nb , which is a consequence of the $N = 50$ and 56 (sub)shell effect.

Figures 7(a) and 7(b) show the excitation energies of the $9/2^+$, $1/2^-$, $3/2^-$, and $5/2^-$ states in $^{89-101}\text{Nb}$ as well as $^{91-103}\text{Tc}$ isotopes. The level structures from $N = 48$ to 60 change rapidly. The large energy gaps between the $9/2^+$

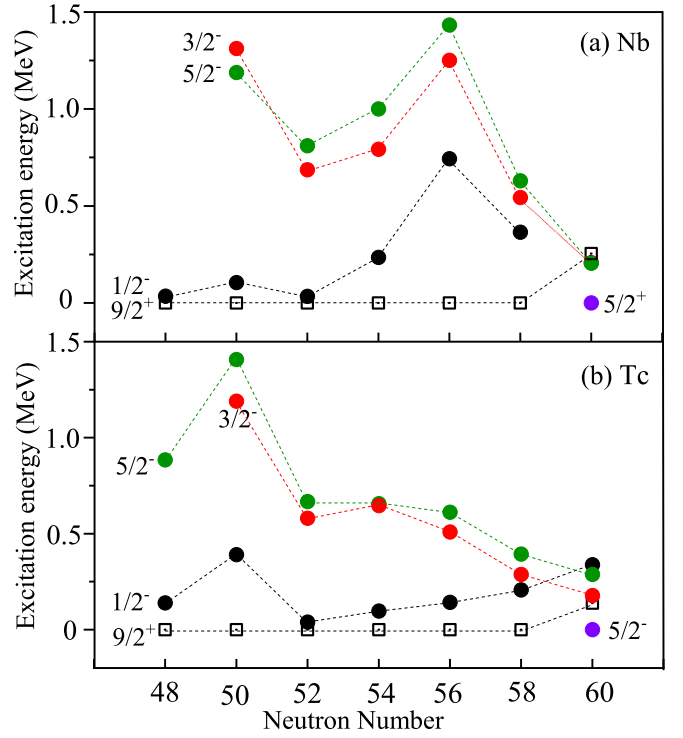


FIG. 7. (a) Comparison of the energy levels $1/2^-$, $3/2^-$, and $5/2^-$ states in Nb isotopes [13,18,31–36]; (b) the same as (a) but for Tc isotopes [21,32–34,37–39].

and the $5/2^-$, $3/2^-$ states in ^{91}Nb as well as ^{97}Nb indicate the stability of the $Z = 38$ (40) subshell at $N = 50$ (56).

In the Nb and Tc isotopes, the ground states show an abrupt change from $9/2^+$ to $5/2^+$ at $N = 60$, which suggests the onset of deformation in ^{101}Nb and ^{103}Tc due to the sudden disappearance of the $Z = 40$ subshell for nuclei with $N \geq 60$. Reference [40] reported that ^{101}Nb has a deformed shape with $\varepsilon_2 \approx 0.37$ and $\gamma \approx -12^\circ$, and the ground-state band can be interpreted by the $5/2^+$ [422] configuration in the Nilsson model.

V. SUMMARY

High-spin states of ^{93}Nb were populated via the reactions $^{82}\text{Se}(^{14}\text{N}, 3n)^{93}\text{Nb}$ and $^{82}\text{Se}(^{16}\text{O}, 1p4n)^{93}\text{Nb}$. The level scheme of ^{93}Nb was extended by adding 13 γ transitions. The observed states were interpreted using the shell model by considering the particle-hole excitation of the $Z = 38$ (40) and $N = 56$ (50) (sub)shell closures. According to the calculated results, the low-lying states can be interpreted as the excitation of the valence protons from the $p_{1/2}$ orbit, across the $Z = 40$ subshell, into the $g_{9/2}$ orbit. The medium spin states, even high-spin states involve not only the proton excitation across the $Z = 38$ (40) subshell ($f_{5/2}p_{1/2}p_{3/2} \rightarrow g_{9/2}$), but also the neutron excitations across the $N = 56$ subshell ($d_{5/2} \rightarrow g_{7/2}$) and $N = 50$ shell closure ($g_{9/2} \rightarrow d_{5/2}, g_{7/2}$).

We study the systematics of low-lying states in the odd-A Nb and Tc isotopes, the even-even Zr isotopes, and the $N = 52$ isotones. We find that the low-lying states of the odd-A nucleus can be regarded as the coupling of a valence nucleon and

its neighboring even-even core. The Zr and Nb isotopes with $N \leq 58$ are nearly spherical nuclei, which are affected by the $Z = 40$ (or 38) subshell. The nuclei with $N \geq 60$ are not affected by the $Z = 40$ subshell, and, thus, lead to deformation.

ACKNOWLEDGMENTS

We would like to acknowledge the excellent work of all the HI-13 tandem accelerator staff for the smooth op-

eration of the machine. We are grateful to Dr. Q. W. Fan for assistance during target preparation. This work was supported by the National Basic Research Programme of China under Grant No. 2007CB815005, the National Natural Science Foundation of China under Grants No. 11075064, No. 11775098, No. 12075169, and No. U1867210, and supported by the National Key R&D Program of China under Grant No. 2018YFA0404403.

-
- [1] Z. G. Wang, M. L. Liu, Y. H. Zhang, X. H. Zhou, S. Guo, J. G. Wang, X. G. Lei, Y. Zheng, Y. D. Fang, Y. H. Qiang, N. T. Zhang, B. Ding, G. S. Li, F. Ma, X. L. Yan, S. C. Wang, B. S. Gao, F. Fang, B. T. Hu, X. G. Wu *et al.*, *Phys. Rev. C* **89**, 044308 (2014).
- [2] Y.-F. Lv, J.-B. Lu, G.-L. Zhang *et al.*, *Chin. Phys. C* **43**, 104102 (2019).
- [3] Y. Zheng, Y. H. Wu, X. G. Wu, C. B. Li, L. H. Zhu, T. X. Li, P. W. Luo, G. S. Li, C. Y. He, H. W. Li, S. P. Hu, J. J. Liu, J. L. Wang, S. H. Yao, Q. M. Chen, J. Zhong, J. B. Lu, K. Y. Ma, and D. Yang, *Phys. Rev. C* **100**, 014325 (2019).
- [4] Z. Q. Li, S. Y. Wang, C. Y. Niu, B. Qi, S. Wang, D. P. Sun, C. Liu, C. J. Xu, L. Liu, P. Zhang, X. G. Wu, G. S. Li, C. Y. He, Y. Zheng, C. B. Li, B. B. Yu, S. P. Hu, S. H. Yao, X. P. Cao, and J. L. Wang, *Phys. Rev. C* **94**, 014315 (2016).
- [5] C. Fransen, N. Pietralla, Z. Ammar, D. Bandyopadhyay, N. Boukharouba, P. von Brentano, A. Dewald, J. Gableske, A. Gade, J. Jolie, U. Kneissl, S. R. Leshner, A. F. Lisetskiy, M. T. McEllistrem, M. Merrick, H. H. Pitz, N. Warr, V. Werner, and S. W. Yates, *Phys. Rev. C* **67**, 024307 (2003).
- [6] Y. H. Zhang, M. Hasegawa, W. T. Guo, M. L. Liu, X. H. Zhou, G. de Angelis, T. M. Axiotis, A. Gadea, N. Marginean, T. Martinez, D. R. Napoli, C. Rusu, Z. Podolyak, C. Ur, D. Bazzacco, F. Brandolini, S. Lunardi, S. M. Lenzi, R. Menegazzo, R. Schwengner, A. Gargano, W. von Oertzen, and S. Tazaki, *Phys. Rev. C* **79**, 044316 (2009).
- [7] E. Galindo, M. Hausmann, A. Jungclaus, K. P. Lieb, O. Yordanov, I. P. Johnstone, R. Schwengner, A. Dewald, A. Fitzler, O. Möller, G. de Angelis, A. Gadea, T. Martinez, D. R. Napoli, and C. A. Ur, *Phys. Rev. C* **69**, 024304 (2004).
- [8] S. S. Ghugre, S. Naguleswaran, R. K. Bhowmik, U. Garg, S. B. Patel, W. Reviol, and J. C. Walpe, *Phys. Rev. C* **51**, 2809 (1995).
- [9] B. Kharraja, S. S. Ghugre, U. Garg, R. V. F. Janssens, M. P. Carpenter, B. Crowell, T. L. Khoo, T. Lauritsen, D. Nisius, W. Reviol, W. F. Mueller, L. L. Riedinger, and R. Kaczarowski, *Phys. Rev. C* **57**, 83 (1998).
- [10] D. Bucurescu, Z. Podolyák, C. Rusu, G. de Angelis, Y. H. Zhang, G. Căta-Danil, I. Căta-Danil, M. Ivaşcu, N. Mărginean, R. Mărginean, L. C. Mihăilescu, G. A. Suliman, P. H. Regan, W. Gelletly, S. D. Langdown, J. J. Valiente Dobón, D. Bazzacco, S. Lunardi, C. A. Ur, M. Axiotis, A. Gadea, E. Farnea, M. Ionescu-Bujor *et al.*, *Phys. Rev. C* **71**, 034315 (2005).
- [11] C. J. Xu, S. Y. Wang, C. Y. Niu, C. Liu, B. Qi, D. P. Sun, L. Liu, P. Zhang, Z. Q. Li, Z. Wang, X. G. Wu, G. S. Li, C. Y. He, Y. Zheng, B. B. Yu, C. B. Li, S. P. Hu, S. H. Yao, X. P. Cao, and J. L. Wang, *Phys. Rev. C* **86**, 027302 (2012).
- [12] R.-J. Guo, Z.-Q. Li, C. Liu, *et al.*, *Chin. Phys. C* **41**, 084105 (2017).
- [13] P. W. Luo, X. G. Wu, H. B. Sun, G. S. Li, C. Y. He, Y. Zheng, C. B. Li, S. P. Hu, Y. H. Wu, H. W. Li, J. J. Liu, J. L. Wang, S. H. Yao, and S. A. Edwards, *Phys. Rev. C* **89**, 034318 (2014).
- [14] A. Chakraborty, Krishichayan, S. S. Ghugre, R. Goswami, S. Mukhopadhyay, N. S. Pattabiraman, S. Ray, A. K. Sinha, S. Sarkar, P. V. Madhusudhana Rao, U. Garg, S. K. Basu, M. B. Chatterjee, M. Saha Sarkar, L. Chaturvedi, A. Dhal, R. K. Sinha, I. M. Govil, R. K. Bhowmik, A. Jhingan, N. Madhavan, S. Muralithar *et al.*, *Phys. Rev. C* **72**, 054309 (2005).
- [15] R. A. Meyer and R. P. Yaffe, *Phys. Rev. C* **15**, 390 (1977).
- [16] T. Hori, T. Masue, A. Odahara, K. Kura, K. Tajiri, T. Shimoda, T. Fukuchi, T. Suzuki, Y. Wakabayashi, Y. Gono, and K. Ogawa, *Phys. Rev. C* **80**, 034306 (2009).
- [17] M. S. Zisman and B. G. Harvey, *Phys. Rev. C* **5**, 1031 (1972).
- [18] J. N. Orce, C. Fransen, A. Linnemann, C. J. McKay, S. R. Leshner, N. Pietralla, V. Werner, G. Friessner, C. Kohstall, D. Mücher, H. H. Pitz, M. Scheck, C. Scholl, F. Stedile, N. Warr, S. Walter, P. von Brentano, U. Kneissl, M. T. McEllistrem, and S. W. Yates, *Phys. Rev. C* **75**, 014303 (2007).
- [19] J. N. Orce, J. D. Holt, A. Linnemann, C. J. McKay, C. Fransen, J. Jolie, T. T. S. Kuo, S. R. Leshner, M. T. McEllistrem, N. Pietralla, N. Warr, V. Werner, and S. W. Yates, *Phys. Rev. C* **82**, 044317 (2010).
- [20] Y. Wakabayashi, T. Fukuchi, Y. Gono *et al.*, *J. Phys. Soc. Jpn.* **76**, 114202 (2007).
- [21] E. A. Stefanova, R. Schwengner, G. Rainovski, K. D. Schilling, A. Wagner, F. Döna, E. Galindo, A. Jungclaus, K. P. Lieb, O. Thelen, J. Eberth, D. R. Napoli, C. A. Ur, G. de Angelis, M. Axiotis, A. Gadea, N. Marginean, T. Martinez, T. Kröll, and T. Kutsarova, *Phys. Rev. C* **63**, 064315 (2001).
- [22] S. S. Ghugre, B. Kharraja, U. Garg, R. V. F. Janssens, M. P. Carpenter, B. Crowell, T. L. Khoo, T. Lauritsen, D. Nisius, W. Reviol, W. F. Mueller, L. L. Riedinger, and R. Kaczarowski, *Phys. Rev. C* **61**, 024302 (1999).
- [23] N. Mărginean, D. Bucurescu, G. Căta-Danil, I. Căta-Danil, M. Ivaşcu, and C. A. Ur, *Phys. Rev. C* **62**, 034309 (2000).
- [24] B. A. Brown and W. D. M. Rae, Nushellx@MSU, MSU-NSCL report **524**, 1–29 (2007).
- [25] E. K. Warburton, J. W. Olness, C. J. Lister, R. W. Zurmühle, and J. A. Becker, *Phys. Rev. C* **31**, 1184 (1985).
- [26] N. Fotiades, J. A. Cizewski, J. A. Becker, L. A. Bernstein, D. P. McNabb, W. Younes, R. M. Clark, P. Fallon, I. Y. Lee, A. O. Macchiavelli, A. Holt, and M. Hjorth-Jensen, *Phys. Rev. C* **65**, 044303 (2002).
- [27] D. Abriola and A. A. Sonzogni, *Nucl. Data Sheets* **109**, 2501 (2008).

- [28] B. Singh and H. U. Zhiqiang, *Nucl. Data Sheets* **98**, 335 (2003).
- [29] B. Singh, *Nucl. Data Sheets* **109**, 297 (2008).
- [30] A. Bödeker, K. P. Lieb, C. J. Gross, M. K. Kabadiyski, D. Rudolph, M. Weiszflog, J. Eberth, H. Grawe, J. Heese, and K.-H. Maier, *Phys. Rev. C* **48**, 1617 (1993).
- [31] S. K. Basu, G. Mukherjee, and A. A. Sonzogni, *Nucl. Data Sheets* **111**, 2555 (2010).
- [32] N. Nica, *Nucl. Data Sheets* **111**, 525 (2010).
- [33] E. Browne and J. K. Tuli, *Nucl. Data Sheets* **145**, 25 (2017).
- [34] J. Blachot, *Nucl. Data Sheets* **83**, 1 (1998).
- [35] P. K. Bindal, D. H. Youngblood, and R. L. Kozub, *Phys. Rev. C* **10**, 729 (1974).
- [36] B. Singh, *Nucl. Data Sheets* **114**, 1 (2013).
- [37] C. M. Baglin, *Nucl. Data Sheets* **114**, 1293 (2013).
- [38] C. M. Baglin, *Nucl. Data Sheets* **112**, 1163 (2010).
- [39] C. M. Baglin, *Nucl. Data Sheets* **110**, 265 (2009).
- [40] S. J. Zhu, Y. X. Luo, J. H. Hamilton *et al.*, *Prog. Part. Nucl. Phys.* **59**, 329 (2007).